Tilted Perpendicular Anisotropy-Induced Spin-Orbit Ratchet Effects

Bin Chen(陈彬)[1], Yuantu Long(龙垣图)[1], Yulin Nie(聂宇林)[1], Ziyu Ling(凌姿瑀)[1], Tianping Ma(马天平)[5], Ruixuan Zhang(张瑞轩)[3], Yizheng Wu(吴义政)[2], Yongming Luo(骆泳铭)[1,4*], and Ningning Wang(王宁宁)[1*]

[1]*School of Electronics and Information Engineering, Hangzhou Dianzi University, Hangzhou 310018, China*
[2]*State Key Laboratory of Surface Physics and Department of Physics, Fudan University, Shanghai 200433, China*
[3]*Research Center for Intelligent Computing Platforms, Zhejiang Laboratory, Hangzhou 311121, China*
[4]*Wenzhou Institute of Hangzhou Dianzi University, Wenzhou 325038, China*
[5]*Anhui Key Laboratory of Magnetic Functional Materials and Devices, School of Materials Science and Engineering, Anhui University, Hefei 230601, China*

(Received 17 April 2024; accepted manuscript online 11 June 2024)

Using micromagnetic simulations, we demonstrate the tilted perpendicular anisotropy-induced spin-orbit ratchet effect. In spin-orbit torque (SOT)-induced magnetization switching, the critical currents required to switch between the two magnetization states (upward and downward magnetization) are asymmetric. In addition, in the nanowire structure, tilted anisotropy induces formation of tilted domain walls (DWs). The tilted DWs exhibit a ratchet behavior during motion. The ratchet effect during switching and DW motions can be tuned by changing the current direction with respect to the tilting direction of anisotropy. The ratchet motion of the DWs can be used to mimic the leaky-integrate-fire function of a biological neuron, especially the asymmetric property of the "potential" and "reset" processes. Our results provide a full understanding of the influence of tilted perpendicular anisotropy on SOT-induced magnetization switching and DW motion, and are beneficial for designs of further SOT-based devices.

DOI: 10.1088/0256-307X/41/7/078501

In magnetic systems, magnetic quasiparticles such as domain walls (DWs) can exhibit asymmetric dynamics when moving in opposite directions, known as the magnetic ratchet effect.[1,2] Ratchet behavior is also observed in systems with asymmetric structures, such as "angelfish", "funnel", or "notch" structures[3–5] or systems with non-uniform coupling strengths.[6] In previous studies, ratchet effects have mainly been investigated using magnetic fields or spin transfer torque (STT) as the driving force; ratchet effects driven by spin-orbit torques (SOTs) have not been thoroughly studied. In contrast to external fields or STT, SOT utilizes the spin current from the spin Hall effects.[7] SOT is more efficient than STT and provides new opportunities for device applications, including SOT-MRAM and racetrack memory.[8,9] Although SOT ratchet effects have been observed in systems including Ta/CoFeB/MgO,[10] W/CoFeB/MgO,[11] Hf/CoFeB,[12] and CoFeB/IrMn,[13] their microscopic origin is not fully understood.[7,14] Understanding the manifestation of SOT-induced ratchet effects is beneficial for device applications.

Tilted perpendicular anisotropy has recently attracted considerable interest as it can promote SOT-induced field-free switching of magnetization, such field-free switching has been demonstrated in systems including $SrIrO_3/SrRuO_3$,[15] $L1_0$-FePt,[16] and CoPt.[17] In this study, using micromagnetic simulations, we show that in systems with tilted anisotropy, ratchet effects can be observed, manifesting as magnetization switching and DW motion. During magnetization switching, the critical currents required to switch from up-to-down to down-to-up are asymmetric. In nanowire structures, tilted anisotropy can lead to the formation of tilted Bloch and Néel walls, depending on the tilting direction of the anisotropy (φ_0) with respect to the nanowire. When driven by SOT, tilted DWs exhibit a ratchet behavior and can be tuned by the current direction with respect to the direction of the anisotropy. The ratchet DW motion can mimic the leaky-integrate-fire function of a biological neuron, especially the asymmetric property of the "potential" and "reset" processes. Our results provide a full understanding of SOT-induced magnetization switching in a system with tilted anisotropy and a new direction for design of spintronic devices.

Ratchet Effects in Magnetization Switching. We first studied the SOT-induced magnetization switching in a system with tilted perpendicular anisotropy. We chose the CoPt/Pt bilayer system as the model system. It has recently been experimentally demonstrated that tilted anisotropy can be realized when CoPt is grown on vicinal Al_2O_3 substrates.[17] In our model, the CoPt film was $200\times50\,(\mathrm{nm}^2)$ and 5 nm in thickness, as shown in Fig. 1(a). The direction of the magnetic easy axis, $\hat{\boldsymbol{e}}_\mathrm{a}$, is defined as $(\varphi_0,\ \theta_0)$, where φ_0 and θ_0 are the angles with respect to the x and z, axes, respectively. The magnetic parameters

*Corresponding authors. Email: ymluo@hdu.edu.cn; ning.wang@hdu.edu.cn
© 2024 Chinese Physical Society and IOP Publishing Ltd

of CoPt and the default parameters used in the simulation are summarized in the Supplementary Information (SI). When current is applied along the x axis, the spin Hall effect in Pt induces a spin current density within the Pt layer such that spin moments pointing in the y direction ($\boldsymbol{\sigma}_y$) flow upward in the z direction. When the spin current flows across the Pt/CoPt interface, the spin current imparts a torque on the CoPt layer, expressed as

$$\boldsymbol{\tau}_{\rm sot} = \tau^0_{\rm sot}(\boldsymbol{m}\times\boldsymbol{\sigma}_y\times\boldsymbol{m}) = \frac{h}{2eM_{\rm S}t}J_{\rm S}(\boldsymbol{m}\times\boldsymbol{\sigma}_y\times\boldsymbol{m}), \quad (1)$$

inducing switching of the CoPt magnetization. Here, $\tau^0_{\rm sot}$ represents the amplitude of SOT; t is the thickness of a CoPt layer; h, e, and $J_{\rm S}$ stands for the Planck constant, elementary charge, and spin current density, respectively. Magnetic fields along the current direction, H_x, are applied to help switching. We did not consider the thermal effects in our simulation. We used the OOMMF code to perform the simulation.

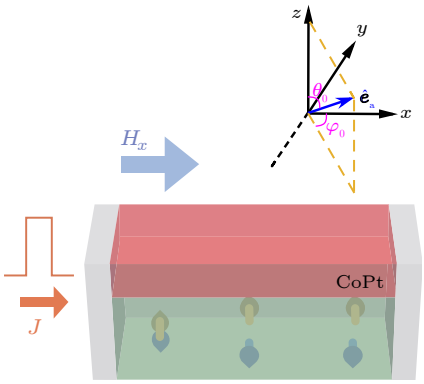

Fig. 1. Schematic of SOT-induced switching in the CoPt/Pt bilayer structure. Here φ_0 and θ_0 are the angles of the easy axis with respect to the x and z axes, respectively. Both the thickness of the CoPt film and the Pt layer are 5 nm. Pulse currents with different amplitudes are applied along the x axis. External fields along the current direction, H_x, are applied.

Figure 2(a) shows the simulation results with the current perpendicular to the tilting plane of the easy axis ($\varphi_0 = 90°$, $\theta_0 = 6°$). Clear switching loops were observed at different H_x values, demonstrating the switching of the CoPt magnetization. The switching polarity was reversed in the direction of H_x, consistent with the typical characteristics of SOT switching in perpendicular magnetization. Switching could still be realized with $H_x = 0$, consistent with the previously reported tilted easy axis-induced field-free switching.[15] For comparison, we simulated the switching behavior when the current was parallel to the tilting plane of the easy axis ($\varphi_0 = 0°$, $\theta_0 = 6°$). The results are presented in Fig. 2(b). There are two differences compared with the case of $\varphi_0 = 90°$. First, switching loops are not observed with $H_x = 0$, indicating that field-free switching could not be realized. Second, the critical switching currents for the upward and downward magnetizations ($J_{\rm C}^+$ and $J_{\rm C}^-$) are asymmetric. Figure 2(b) shows that $J_{\rm C}^+$ and $J_{\rm C}^-$ are 8.1×10^{12} and 10.6×10^{12} A/m^2, respectively, when $H_x = 400$ Oe. This means that it is easier for the magnetization to switch from downward to upward, demonstrating the ratchet effect during switching. In our control experiments, we found that the switching asymmetry $\Delta J = |J_{\rm C}^-| - |J_{\rm C}^+|$ increases with the tilt angle θ_0 and does not exist in a system with perpendicular anisotropy ($\theta_0 = 0°$) (as shown in the SI). This indicates that tilted anisotropy is the direct origin of the ratchet effect. Figure 2(c) plots the switching currents ($J_{\rm C}^+$ and $J_{\rm C}^-$) and the switching asymmetry ΔJ as functions of H_x. $J_{\rm C}^+$ and $J_{\rm C}^-$ decrease with the amplitude of H_x, whereas ΔJ increases with H_x, indicating that H_x plays a critical role in ratchet effects. We also demonstrated that the field-like torque $\boldsymbol{\tau}_{\rm FL} \propto \boldsymbol{m}\times\boldsymbol{\sigma}_y$ only influences the switching current and cannot produce the ratchet effect (as shown in the SI), indicating that the ratchet effect originates from the damping-like torque.

Such ratchet effects can be understood analytically using a microspin model with the magnetization rotated uniformly.[18] The magnetization $\boldsymbol{m}$ is balanced by different torques from SOT, the anisotropy, and the external field. The equilibrium state of the magnetization satisfies the condition $\boldsymbol{\tau}_{\rm sot} + \boldsymbol{\tau}_{\rm ext} + \boldsymbol{\tau}_{\rm an} = 0$, where the torques from the anisotropy and the external field are written as $\boldsymbol{\tau}_{\rm an} = \boldsymbol{m}\times\boldsymbol{B}_{\rm an} = \boldsymbol{m}\times[-B^0_{\rm an}(\boldsymbol{m}-m_z\hat{\boldsymbol{e}}_{\rm a})] = \boldsymbol{m}\times[B^0_{\rm an}m_z\hat{\boldsymbol{e}}_{\rm a}]$ and $\boldsymbol{\tau}_{\rm ext} = \boldsymbol{m}\times\boldsymbol{B}_{\rm ext}$, respectively. Here, $\hat{\boldsymbol{e}}_{\rm a}$ is the unit vector of the easy axis. $B^0_{\rm an}$ and $B_{\rm ext}$ are the amplitudes of the anisotropy field and the external field, respectively. For currents corresponding to small moderate values of spin torque ($|\tau^0_{\rm sot}| < 0.5B^0_{\rm an}$), the tilting direction of easy axis is parallel to the current ($\varphi = 0°$), the external field $\boldsymbol{B}_{\rm ext}$ is limited in the x direction and the magnetization $\boldsymbol{m}$ remains within the xoz plane.[18] We can express the torque balance equation that determines the magnetization rotation angle θ in a simple one-dimensional scalar form:

$$\tau^0_{\rm sot}+B_{\rm ext}\sin(\theta-\beta-\theta_0)-B^0_{\rm an}\sin(\theta-\theta_0)\cos(\theta-\theta_0) = 0, \quad (2)$$

where θ represents the angle between the magnetic moments $\boldsymbol{m}$ and $\boldsymbol{x}$, β represents the angle between the external magnetic fields $\boldsymbol{B}_{\rm ext}$ and $\boldsymbol{x}$. We numerically solved the equation and plotted the equilibrium m_Z as a function of the normalized SOT ($\tau_{\rm sot}/B^0_{\rm an}$) within the range $[-0.5, 0.5]$, as shown in Fig. 2(d). The results show that the switching loop is asymmetric when $\theta_0 \neq 0°$, and is proportional to θ_0, which is in accordance with the simulation results, verifying the physical origin of the ratchet effect. Our results provide a possible explanation for the ratchet effects observed in previous studies on Ta/CoFeB/MgO,[10] W/CoFeB/MgO,[11] and Hf/CoFeB.[12] In these systems, the easy axis of the magnetic layer may be tilted due to competition between demagnetization and interface perpendicular anisotropy.

Comparison of Fig. 2(a) and 2(b) indicates that the field-free switching [Fig. 2(a)] and the ratchet effect [Fig. 2(b)] are competing effects that can be tuned by φ_0. Figure 2(e) shows φ_0 dependence of the switching behavior when $H_x = 0$. When $\varphi_0 > 0°$, clear switching loops are observed. The switching currents ($J_{\rm C}^+$, $J_{\rm C}^-$) are asymmetric

and change with φ_0, indicating the coexistence of field-free switching and ratchet effects. To qualitatively characterize these competing effects, Fig. 2(f) plots the switching currents (J_C^+, J_C^-) and ΔJ as functions of φ_0. The switching current exhibits four-fold symmetry. The results show that as φ_0 increases from 0° to 90°, the critical switching currents (J_C^+, J_C^-) decrease continuously. The switching asymmetry ΔJ decreases continuously with an increase in φ_0. This means that the ratchet effect disappears when φ_0 approaches 90°. The field-free ratchet effect is optimized at $\varphi_0 = 45°$, 135°, 225°, 315°, where the switching and the ratchet effects are balanced. Our results provide a full understanding of the angular dependence of SOT-induced magnetization switching in a system with tilted anisotropy. Moreover, as the requirement of the on-chip magnetic field adds to the complexity of the device structure and operation and is not suitable for real industry application, similar to the intensive pursuit of the "field-free switching" for the development of the SOT-MRAM, the field-free ratchet is also critical for its application in future spintronics.

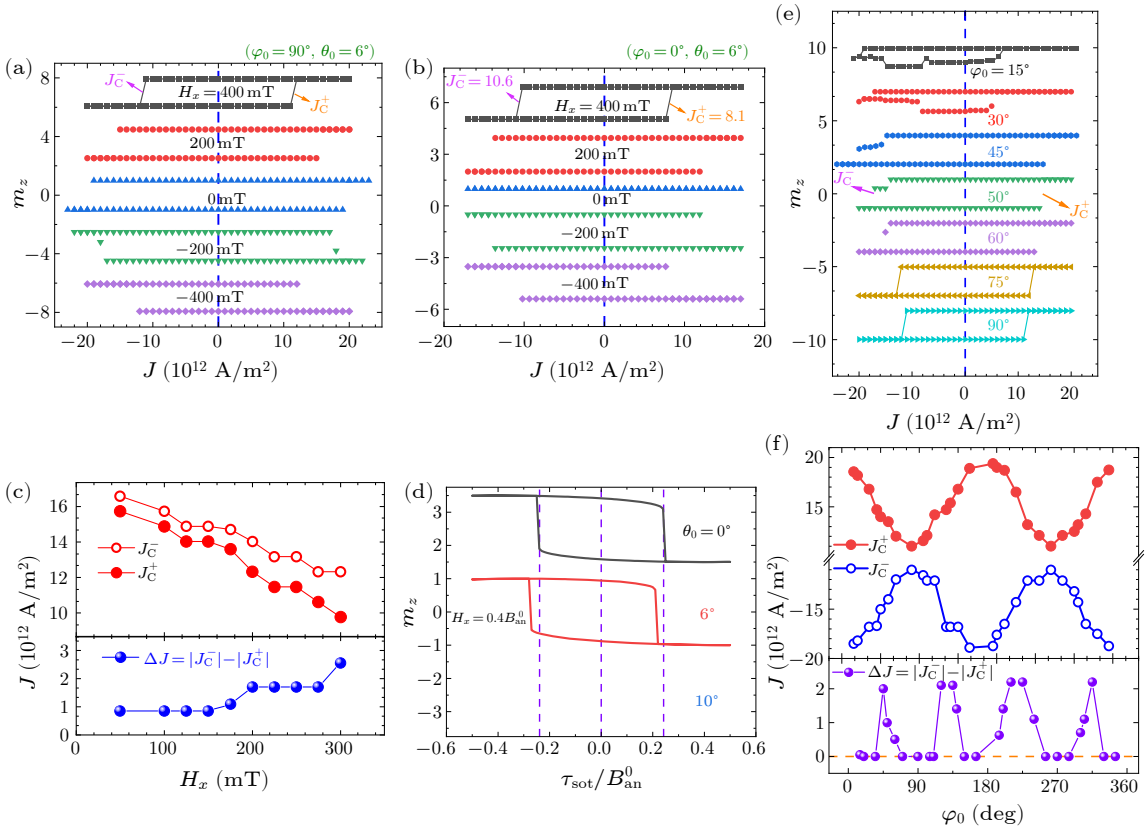

Fig. 2. [(a), (b)] The SOT-induced magnetization switching in the CoPt/Pt film with $\varphi_0 = 0°$ and 90°, respectively. The switching loops at different H_x are offset for clarity. J_C^+ and J_C^- represent the thresholds of the switching current density for the positive and negative currents, respectively. (c) J_C^+, J_C^-, and ΔJ as functions of H_x when $\varphi_0 = 0°$. (d) The macrospin model results of SOT switching with different θ_0. Here φ_0 is fixed at 0°; H_x is fixed at $0.4B_{an}^0$. (e) The φ_0 dependence of the SOT-induced magnetization switching in the CoPt film with $H_x = 0$. The switching loops at different φ_0 are offset for clarity. (f) J_C^+, J_C^- (top panel), and ΔJ (bottom panel) as functions of φ_0. In (a), (b), (c), (e), and (f), θ_0 is fixed at 6°.

Magnetic Ratchet Effects in DW Motion. In addition to magnetization switching, we investigated SOT-driven DW motion in systems with tilted anisotropy. We simulated DW motion in a CoPt/Pt nanotrack with tilted anisotropy in a system with sizes of 2000 nm × 100 nm × 10 nm, as shown in Fig. 3(a). The easy axis direction is defined as (φ_0, θ_0). To focus on the influence of the tilted easy axis, we did not consider the Dzyaloshinskii–Moriya interaction (DMI) field in our system. According to the tilting plane of the easy axis with respect to the nanowire, two types of DW can typically be formed. A Néel (Bloch) wall can be formed when the tilting plane of the easy axis is parallel (perpendicular) to the nanowire $\varphi_0 = 0°$ ($\varphi_0 = 90°$), as shown in Fig. 3(b). Unlike the DW in the system with a perpendicular easy axis, where the magnetization at the center of the DW ($\boldsymbol{m}_{DW}$) is fully in-plane, in systems with a tilted easy axis, $\boldsymbol{m}_{DW}$ is tilted from the in-plane direction (along the hard axis) and can be considered as a tilted DW. Hybrid DWs can be formed when $0° < \varphi_0 < 90°$; the in-plane component of $\boldsymbol{m}_{DW}$ contains both x and y components. In the following, we discuss the unique dynamics of different types of tilted DWs.

We first studied the SOT-driven motion of the tilted Néel wall. When the tilting plane of the easy axis is parallel to the nanowire ($\varphi_0 = 0°$), the tilted angle is fixed at $\theta_0 = 20°$. The left panel of Fig. 3(c) shows

the DW velocities when driven by positive and negative currents ($\pm 0.8 \times 10^{12}$ A/m^2), with H_x fixed at -35 mT. The results show that the DW velocity V is asymmetric when driven by currents with opposite directions. The DW velocities are 56 m/s for $J = +0.8 \times 10^{12}$ A/m^2, and 30.7 m/s for $J = -0.8 \times 10^{12}$ A/m^2. The existence of $\Delta V = |V_{J+}| - |V_{J-}|$ demonstrates the ratchet effect during DW motion. The DW velocity asymmetry ΔV is proportional to the amplitudes of the current densities, as shown in the right panel of Fig. 3(c). This is in direct contrast to conventional Néel walls in systems with perpendicular anisotropy, in which the velocity is symmetric ($\Delta V = 0$) when driven by currents in opposite directions.[9,19] Our control experiments show that the velocity asymmetry ΔV increases with the tilting angle θ_0, verifying the physical origin of the ratchet effect (shown in the SI).

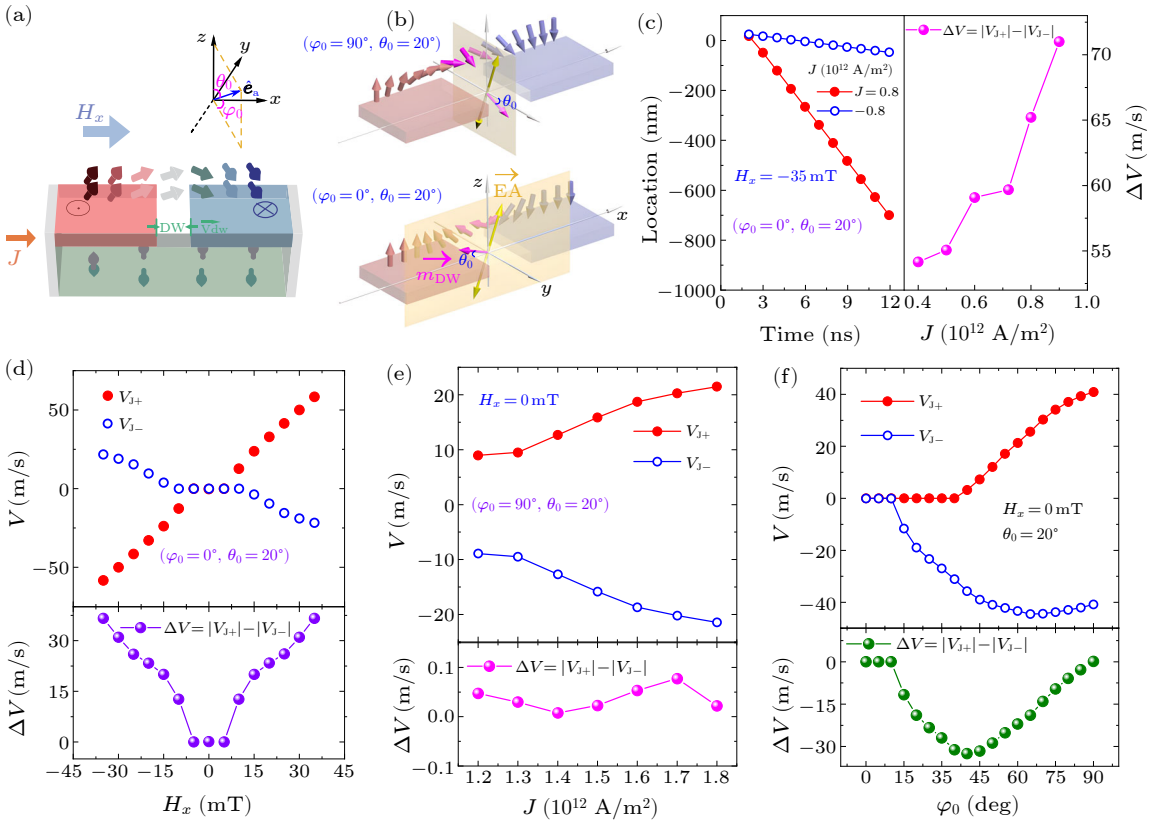

Fig. 3. (a) Schematic of SOT-induced DW motion in the CoPt/Pt nanowire with tilted anisotropy. (b) Formation of two different DW structures: tilted Bloch and Néel walls when $\varphi_0 = 90°$ and $\varphi_0 = 0°$, respectively. Here $\boldsymbol{m}_{DW}$ is tilted from the in-plane direction. (c) Simulation of the current-induced motion of the tilted Néel DW. The left panel shows the DW position as a function of time when driven by currents with different directions ($\pm 8 \times 10^{11}$ A/m^2); H_x is fixed at -35 mT. The right panel shows $\Delta V = |V_{J+}| - |V_{J-}|$ as a function of the current densities. (d) The top panel shows the DW velocity (V_{J+}, V_{J-}) as a function of H_x; the bottom panel shows ΔV as a function of H_x. The amplitude of the current density is fixed at 2.9×10^{12} A/m^2. (e) Simulation of the current-induced motion of the tilted Bloch DW ($\varphi_0 = 90°$). The top and bottom panels show the DW velocities V_{J+}, V_{J-}, and ΔV as functions of current density, with $H_x = 0$. (f) V_{J+}, V_{J-}, and ΔV as functions of φ_0 in the absence of an external field ($H_x = 0$). In (b)–(f), θ_0 is fixed at 20°.

The top and bottom panels in Fig. 3(d) show the DW velocities (V_{J+}, V_{J-}) and ΔV as functions of H_x when driven by currents in opposite directions (2.9×10^{12} A/m^2). The results show that both the velocities (V_{J+} and V_{J-}) and ΔV are nearly proportional to H_x. Because H_x can change the internal spin structure of the DW ($\boldsymbol{m}_{DW}$), the influence of H_x indicates that $\boldsymbol{m}_{DW}$ can play a critical role in DW dynamics. The influence of H_x on ΔV can be explained as follows. In a system with a tilted easy axis, $\boldsymbol{m}_{DW}$ of the Néel wall is tilted away from the x direction, and the z component exists, as shown in Fig. 3(b). Application of H_x forces $\boldsymbol{m}_{DW}$ to return to the in-plane direction (x direction), which breaks the symmetry of the DW magnetization with respect to the hard axis. The tilting of $\boldsymbol{m}_{DW}$ from the hard axis makes it easier to switch to one circumferential direction (upward or downward) using in-plane polarized spin currents, which manifests as the ratchet effect during DW motion. Because the ratchet effect is proportional to the tilting of $\boldsymbol{m}_{DW}$, the ratchet (ΔV) increases with H_x.

Next, we study the SOT-driven motion of a tilted Bloch wall with the tilting plane of the easy axis perpendicular to the direction of the nanowire ($\varphi_0 = 90°$, $\theta_0 = 20°$). For a conventional Bloch wall in FM/HM bilayer systems, it is established that the Bloch DW cannot be driven by spin current induced by the spin Hall effects. To move the

DW, H_x or DMI fields are required.[9] However, this is not the case for tilted Bloch walls in systems with tilted easy axis. Figure 3(e) plots (V_{J+}, V_{J-}) and ΔV as functions of current density with $H_x = 0$ and without DMI. The results show that the tilted DW can be moved by the current, in direct contrast to the conventional Bloch DW. Our control experiments show that the DW velocity increases with the tilting angle θ_0, demonstrating that the DW motion originates from tilting the easy axis. In addition, Fig. 3(e) shows that ratchet effects do not exist ($\Delta V \approx 0$), unlike with $\varphi_0 = 0°$. The motion of the tilted Bloch wall when $H_x = 0$ can be explained as follows. For a conventional Bloch wall, $\boldsymbol{m}_{\rm DW}$ is parallel to the y axis, which is parallel to the polarization direction of the spin current, leading to the disappearance of $\boldsymbol{\tau}_{\rm sot}$, as $\boldsymbol{\tau}_{\rm sot} \propto \boldsymbol{m}_{\rm DW} \times (\boldsymbol{\sigma}_y \times \boldsymbol{m}_{\rm DW})$. When the Bloch wall is tilted, $\boldsymbol{m}_{\rm DW}$ is tilted toward the z axis, which leads to a nonzero $\boldsymbol{\tau}_{\rm sot}$. The $\boldsymbol{\tau}_{\rm sot}$ rotates the $\boldsymbol{m}_{\rm DW}$ toward the y axis, inducing DW motion.

Finally, we investigate the dynamics of a hybrid DW using $0° < \varphi_0 < 90°$ and $\theta_0 = 20°$. The hybrid DW contains both Néel and Bloch components. Thus, its dynamics simultaneously exhibits characteristics of tilted Bloch and Néel DWs. Figure 3(f) shows the dependence of V_{J+}, V_{J-}, and ΔV on φ_0 for $H_x = 0$. When $0° < \varphi_0 < 90°$, the DW can be driven into motion, and there is a nonvanishing ΔV, demonstrating that the motion of the hybrid DW contains characteristics of a tilted Bloch and Néel DW simultaneously. The velocity and ratchet effects are tuned using φ_0. When φ_0 increases from 0° to 90°, the DW velocity increases with φ_0. The ratchet effect is optimized at $\varphi_0 = 45°$ due to competition between the Néel and Bloch components of the hybrid DW. The ratchet effect decreases with an increase in φ_0; the DW velocities increase with φ_0.

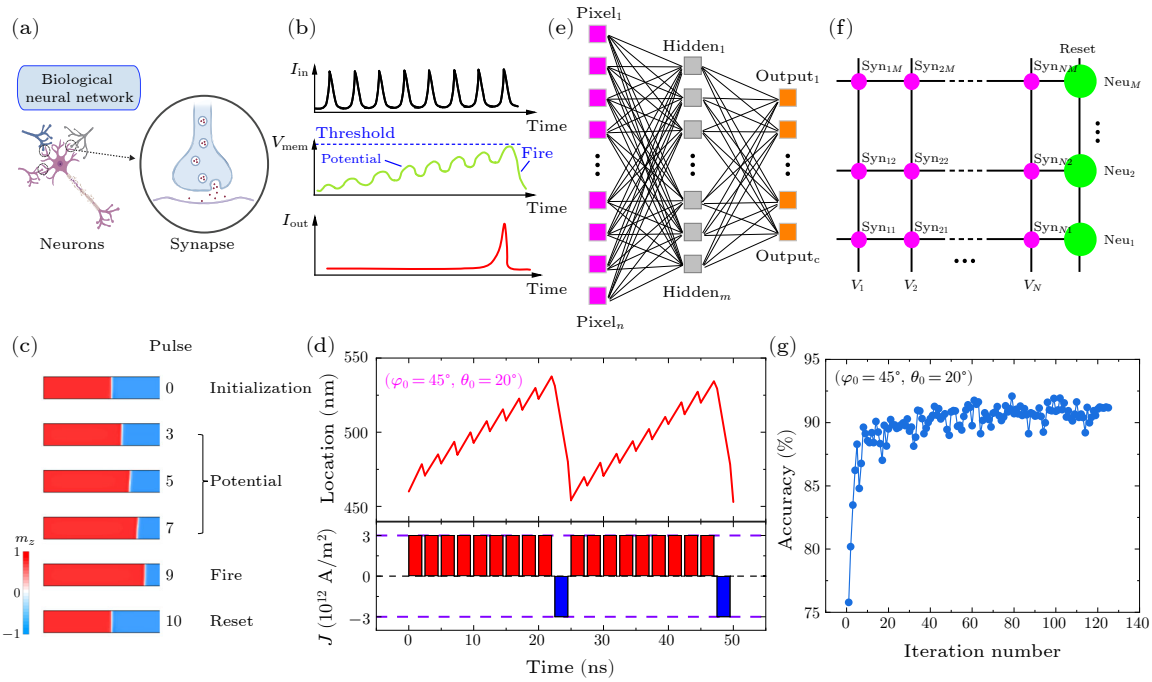

Fig. 4. (a) Illustration of the synaptic structure of a biological neuron. (b) LIF behaviors in the synapse. [(c), (d)] Pulse-current driven DW motion in a system with tilted easy axis. The easy axis direction is $\varphi_0 = 45°$, $\theta_0 = 20°$. (c) Selected snaps of the DW position as a function of time when driven by pulsed currents. (d) The top panel shows the DW position as a function of time when driven by the current sequences shown in the bottom panel. (e) Schematic of the three-layer ANN for the digit-recognition task. (f) Schematic of the proposed crossbar array architecture for the DW synapse and neuron integrated neuromorphic system. (g) Accuracy curve for the pattern-recognition task performed by the neural network with the number of iterations.

Application in Neuromorphic Computing. The ratchet motion of a tilted DW can be used for brain-inspired computations. As shown in Fig. 4(a), the communication between neurons in biological organisms is recognized as the leaky-integrate-fire (LIF) process occurring in the synapse. As shown in Fig. 4(b), with an increase in stimulation, the membrane potential of the synapse continuously accumulates and eventually reaches the threshold (known as the potential process), at which the synapse fires an output spike and then resets to its initial state (known as the "fire and reset" process).[20,21] As shown in Fig. 4(b), the potential and the reset are asymmetric. The potential requires many intermediate states, whereas the reset should be as quick as possible, with no intermediate states. Although previous results have shown that DW motion can be used to mimic LIF functionality using the moving distance of the DW to represent the membrane potential of biological neurons,[22] it cannot accurately describe the asymmetric behavior of the potential and the reset processes. A large current pulse is required for the reset process.[20] We demonstrate that this problem can be avoided by using the ratchet motion of the tilted DW.

Figures 4(c) and 4(d) show the SOT-driven DW motion in a system with tilted anisotropy ($\varphi_0 = 45°$ and

$\theta_0 = 20°$). Pulse currents with 3×10^{12} A/m^2 and a duration of 2 ns are used to drive the DW motion. As shown in Fig. 4(c), with application of positive current pulses, the DW gradually moves from the center to the right and returns to its initial position when a negative current pulse is applied. Figure 4(d) shows the DW position as a function of the current pulses. Owing to the ratchet effect, nine positive pulses are required to drive the DW from the center to the right edge; one negative pulse is required to drive the DW to return to the initial position. DW motion driven by a positive current with more intermediate states could mimic the long-term potentiation (LTP) process; the motion driven by negative current could represent the short-term fire and reset process. This behavior mimics the LIF functionality of biological neurons. During the reset process, only one pulse with the same amplitude and duration is required. This means that the fire-and-reset process is much quicker and more energy efficient than that with conventional perpendicular easy axis, where a much larger current pulse is required for the reset process,[20] demonstrating the advantage of the ratchet DW motion-based neuron.

To verify the performance of our DW neurons, we constructed and simulated a three-layer artificial neural network (ANN), and performed the MNIST handwritten digit recognition task, as described in Ref. [23]. The working principle of the recognition process is described as follows: 28×28 pixels^2 of an input handwritten digital image were converted into 784 voltage signals that were input into the network. The three-layer ANN contained 784, 100, and 10 neurons in the input, hidden, and output layers, respectively. The ten output neurons corresponded to output numbers ranging from zero to nine, as shown in Fig. 4(e). For each neuron, the LIF behavior of the DW neuron was simulated using the characteristic data in Fig. 4(d). The DW neuron comprised a three-layer algorithm with 784 neurons in the input layer, 100 neurons in the hidden layer, and 10 neurons in the output layer, resulting in an N × M synapse matrix, as shown in Fig. 4(f). In the matrix, the input voltages $V_{\rm i}$ are applied to Syn$_{ij}$, where i is the row number and j is the column number. The integration of Syn$_{ij}$ is sent to Neu$_j$; the output comes from the nonlinear process of Neu$_j$ signals in the order of $V_{\rm i}$ to Syn$_{ij}$ to Neu$_j$ logic, as shown in Fig. 4(f). As the writing pulse voltage was applied to each neural device, the DW motion led to different electrical states in Syn$_{ij}$. The voltages and currents were summed and transformed into the artificial neuron Neu$_j$ with distribution of the normalized pulse voltage. A modified SIGMOD function was used to fit the characteristics of the data shown in Fig. 4(d); 60000 training images and 10000 testing images are used in the MNIST dataset, with normalized weights from −1 to 1. The learning rate for the hidden layer is 0.4 and for the output layer is 0.2. Figure 4(g) shows the accuracy of the ANN for the MNIST handwritten-digit recognition task as a function of the number of iterations. The results show that the DW neuron-based ANN achieves a recognition accuracy greater than 93%, similar to that of the magnetic neuron-based ANN.[24,25]

In summary, we have studied the SOT-induced ratchet effect in systems with tilted anisotropy. The ratchet effect is present during magnetization switching and manifested as DW motion, which has not been fully recognized. Our results provide a complete understanding of the influence of tilted easy axis on switching and DW motion. We demonstrate that the ratchet effect can be used in neuromorphic computing, and has an advantage during the reset process.

Acknowledgements. This work was supported by the National Natural Science Foundation of China (Grant No. 12274108), the Natural Science Foundation of Zhejiang Province (Grant Nos. LY23A040008 and LY23A040008), and the Basic Scientific Research Project of Wenzhou (Grant No. G20220025).

References

[1] Souza J C B, Vizarim N P, Reichhardt C J O *et al.* 2021 *Phys. Rev. B* **104** 054434
[2] Migita K, Yamada K, and Nakatani Y 2020 *Appl. Phys. Express* **13** 73003
[3] Franken J H, Swagten H J M, and Koopmans B 2012 *Nat. Nanotechnol.* **7** 499
[4] Yamaguchi R, Yamada K, and Nakatani Y 2021 *Jpn. J. Appl. Phys.* **60** 10904
[5] Wang J L, Xia J, Zhang X C *et al.* 2020 *Appl. Phys. Lett.* **117** 202401
[6] Lavrijsen R, Lee J H, Fernández-Pacheco A *et al.* 2013 *Nature* **493** 647
[7] Liu L Q, Pai C F, Li Y *et al.* 2012 *Science* **336** 555
[8] Ramaswamy R, Lee J M, Cai K M, and Yang H 2018 *Appl. Phys. Rev.* **5** 31107
[9] Haazen P P J, Murè E, Franken J H *et al.* 2013 *Nat. Mater.* **12** 299
[10] Hao Q and Xiao G 2015 *Phys. Rev. B* **91** 224413
[11] Hao Q and Xiao G 2015 *Phys. Rev. Appl.* **3** 034009
[12] Torrejon J, Garcia-Sanchez F, Taniguchi T *et al.* 2015 *Phys. Rev. B* **91** 214434
[13] Huang Y H, Yang C Y, Cheng C W *et al.* 2022 *Adv. Funct. Mater.* **32** 2111653
[14] Zhu L 2023 *Adv. Mater.* **35** 2300853
[15] Liu L, Qin Q, Lin W N *et al.* 2019 *Nat. Nanotechnol.* **14** 939
[16] Luo Y M, Zhuang Y S, Feng Z S *et al.* 2022 *Front. Phys.* **17** 53511
[17] Luo Y M, Liang M F, Feng Z S *et al.* 2023 arXiv:2306.02616 [cond-mat.mtrl-sci]
[18] Liu L Q, Lee O J, Gudmundsen T J *et al.* 2012 *Phys. Rev. Lett.* **109** 96602
[19] Ryu K S, Thomas L, Yang S H *et al.* 2013 *Nat. Nanotechnol.* **8** 527
[20] Li S, Kang W, Huang Y Q *et al.* 2017 *Nanotechnology* **28** 31LT01
[21] Prezioso M, Merrikh-Bayat F, Hoskins B D *et al.* 2015 *Nature* **521** 61
[22] Lequeux S, Sampaio J, Cros V *et al.* 2016 *Sci. Rep.* **6** 31510
[23] Chen P Y, Peng X, and Yu S 2017 *IEEE Int. Electron Devices Meeting (IEDM)*, 2–6 December 2017, San Francisco, CA, USA, p. 6.1.1
[24] Liu J H, Xu T, Feng H M *et al.* 2022 *Adv. Funct. Mater.* **32** 2107870
[25] Song K M, Jeong J S, Pan B *et al.* 2020 *Nat. Electron.* **3** 148